ChemPubSoc Europe

DOI: 10.1002/cphc.201500854

CHEMPHYSCHEM Articles

VIP *Very Important Paper*

Electrochemical Biosensor Based on Nanoporous Au/CoO Core–Shell Material with Synergistic Catalysis

Chao Zhang,[a] Bin Huang,[b] Lihua Qian,*[a] Songliu Yuan,[a] Shuai Wang,[c] and Rong Chen*[b]

An ultrathin CoO layer is deposited on the skeleton surfaces of a nanoporous gold (NPG) film by using atomic layer deposition, creating a flexible electrode. Detailed characterization demonstrates the superior performance of the flexible NPG/CoO hybrids for electrochemical catalysis. The NPG/CoO hybrid not only achieves high catalytic activity for glucose oxidation and H_2O_2 reduction, but also exhibits a linear dependence of the electrical signal on the concentration of glucose and H_2O_2 molecules in the electrolyte. Meanwhile, the sensitivity for H_2O_2 reduction can be as high as 62.5 $\mu A\,mM^{-1}\,cm^{-2}$ with linear dependence on the concentration in the range of 0.1–92.9 mM. The high sensitivity is proposed to result from the synergistic effect of Au and CoO at the interfaces, and the high conductivity of the gold skeleton with a large surface area. The superior electrochemical performance of this hybrid electrode is promising for future potential applications in various transitional-metal-oxide-based electrochemical electrodes.

1. Introduction

The meticulous configuration of heterogeneous interfaces usually bestows condensed matters upon some novel and versatile performances. Photocatalysis[1–3] and electrochemical catalysis[4–6] are experimentally investigated at many heterogeneous interfaces, including metal/transition-metal oxide,[1] graphene/transition-metal oxide,[2,5] carbon nanotube/transition-metal oxide,[3,6] etc. These hybrid nanostructures can naturally hold multiple functions, relying on the tunable compositions and morphologies of multiple components. Most importantly, electron transfer and band offset at the heterogeneous interfaces can cause some synergistic performances that often exhibit a superior performance compared to each component or cannot be observed in each isolated component.[7,8] Stimulated by the demands of green energy and flexible devices in the past decade, heterogeneous interfaces consisting of noble metals and transition-metal oxides have widely been utilized as electrodes.[9,10] Most transition-metal oxides, such as RuO_2,[11] NiO,[12] Co_3O_4,[13,14] CuO,[15] and CoO[16] are redox active, such that they are potential candidates as electrodes in ultrasensitive electrochemical sensors. Among them, cobalt oxides including Co_3O_4 and CoO are attractive materials, owing to their microstructure stabilities in alkaline conditions, excellent electrocatalytic activity, and variable valence states.

Essentially, both mass transport and electron transport within the hybrid nanostructures become crucial issues in obtaining excellent electrocatalytic properties. Usually, cobalt oxides with different morphologies are fabricated by using various approaches including chemical synthesis, hydrothermal synthesis, chemical vapor deposition, and so forth. A large fraction of hollow channels embedded within these hybrid nanostructures can benefit the entrance and outflow of electrolytes, resulting in favorable kinetics during electrochemical catalysis.[17,18] To enhance the effective transport of electrolytes and redox kinetics at metal/oxide interfaces, hierarchical nanoporous structures have also been reliably fabricated. On the other hand, carbon-incorporated networks including carbon nanotubes, graphene nanosheets, and carbon cloth exhibit excellent conductivity, such that they can serve as efficient current collectors when their surface is functionalized with cobalt oxides, resulting in synergistic catalysis at the interfaces.[19] Except for carbon-incorporated networks, nanoporous metals with superior conductivity are also considered as the approximate candidates for electrochemical electrodes.[20] Nanoporous metals decorated with transition-metal oxides have emerging applications in electrochemical catalysis.[13] Nanoporous metals have rigid skeletons with ultrahigh mechanical strength, which can avoid the random aggregations and catastrophic collapse of metal oxides in favor of stable mass transport within the porous channels during electrochemical reactions.[21–23] Meanwhile, excellent conductivity can significantly decrease the internal resistance of the hybrid electrode, which is in favor of improving the efficiency of the electrochemical reaction. Free-standing nanoporous gold (NPG) films have been experimen-

[a] C. Zhang, Prof. L. Qian, Prof. S. Yuan
School of Physics
Huazhong University of Science and Technology
1037 Luoyu Road, Hongshan District, Wuhan, 430074 (China)
E-mail: lhqian@hust.edu.cn

[b] B. Huang, Prof. R. Chen
School of Mechanical Science and Engineering
Huazhong University of Science and Technology
1037 Luoyu Road, Hongshan District, Wuhan, 430074 (China)
E-mail: rongchen@mail.hust.edu.cn

[c] Prof. S. Wang
School of Chemistry and Chemical Engineering
Huazhong University of Science and Technology
1037 Luoyu Road, Hongshan District, Wuhan, 430074 (China)

Supporting Information for this article is available on the WWW under http://dx.doi.org/10.1002/cphc.201500854.

tally demonstrated as high-performance catalysts for methanol oxidation in alkaline solution,[24] and the aerobic oxidation of glucose to gluconic acid under mild condition.[25]

However, to further improve the synergistic effect occurring at the heterogeneous interfaces between nanoporous Au and cobalt oxides, more precise manipulation over the interfaces at nanometer, or even atomic scales becomes the crucial concern in terms of high-performance electrodes and om clarifying the intrinsic mechanism of the catalytic abilities. This conception for nanoporous metal/transition-metal oxides can provide vast opportunities to promote the optimal electrode design in electrochemical catalysis. In this paper, we fabricate the NPG/CoO hybrid as a flexible electrode by means of atomic layer deposition (ALD), as illustrated in Figure 1. Owing to the ability to

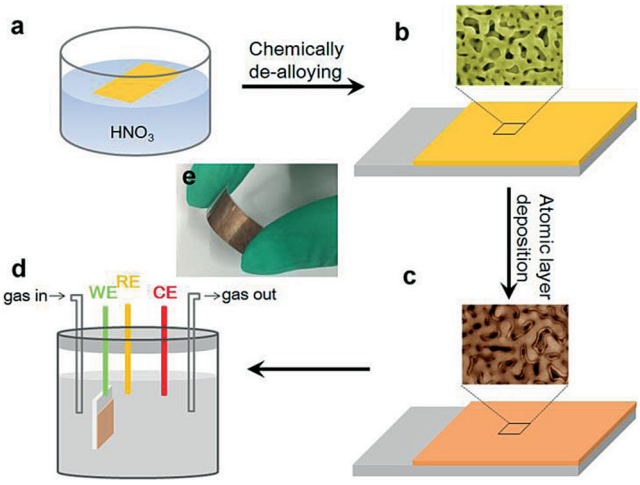

Figure 1. Fabrication of NPG/CoO hybrid electrodes. a) Free-standing NPG is fabricated by de-alloying a commercial $Au_{35}Ag_{65}$ film in concentrated HNO_3 solution; b) the NPG is fixed onto the PET as a flexible electrode; c) CoO films are decorated onto nanoporous channels of NPG by using the ALD method; d) the NPG/CoO electrode was tested in a three-electrode system; e) demonstration of the flexibility of NPG/CoO electrode.

tailor the geometrical scale of cobalt oxides shell at the atomic scale, the NPG/CoO hybrid can serve as model architecture to investigate its synergistic catalysis experimentally. The NPG skeleton, anchored on tiny cobalt oxide nanoparticles or an ultrathin film, acts as a highly active material for electrocatalysis.

2. Results and Discussion

Figures 2a and 2b show the surface morphologies of the nanoporous NPG/CoO hybrid electrodes after ALD for 100 and 200 cycles, respectively. The interconnected network is the Au skeletons, with nanoporous channels with a characteristic length of 40–100 nm. By increasing the deposition cycles, the loading mass or the nominal thickness of the CoO layer [detailed analysis of the element composition can be confirmed by using energy-dispersive X-ray spectroscopy (EDS) and X-ray photoelectron spectroscopy (XPS) analysis] shows monotonic increment. When the number of deposition cycles is less than 200, CoO products prefer to be in the discontinuous layer, so

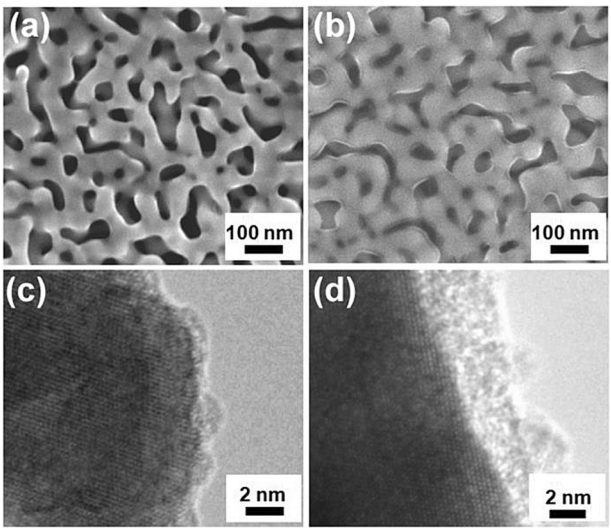

Figure 2. SEM images of NPG films after CoO deposition for a) 100 and b) 200 cycles, and the corresponding high-resolution TEM images of NPG/CoO films after CoO deposition for c) 100 and d) 200 cycles, illustrating the amorphous CoO uniformly covering the gold skeletons.

that some islands are anchored onto the Au ligament, as shown in Figure 2c. However, an almost continuous CoO layer can be observed, as shown in Figure 2d, with further ALD. The high-resolution transmission electron microscopy (HRTEM) image demonstrates that the CoO shell is in an amorphous state. Meanwhile, the uniform deposition of the CoO shell onto the Au ligament can ensure chemical bonding interfaces between the Au core and the CoO shell, as shown in Figures 2c and 2d, such that the NPG/CoO hybrid offers excellent electrochemical performances, which stem from the superior conductivity of the interconnected Au skeletons and synergistic catalysis occurring at the abundant Au/CoO interfaces, as discussed later. With increasing number of depositing cycles, the CoO shell covering the surface of nanoporous Au skeletons gets thicker and thicker (Figure S1). Owing to the geometrical confinement of the pores during ALD, Au skeletons at the bottom [at the polyethylene terephthalate (PET) side] cannot be covered by the CoO. So, the catalytic activity should be attributed to the bare Au skeletons at the bottom and the CoO covering gold skeleton at the top, such that the catalytic activity can be attributed to both the bare Au skeletons and CoO shell, as shown in Figure S2. Besides the surface morphologies, detailed information on the compositions and chemical bonds can be further characterized by using EDS and XPS. Atomic percentages of Co and O elements are determined by quantitatively analyzing the EDS spectrum in Figure S3a, and the corresponding values of 1.58 and 52.57% indicate the formation of CoO products. Elemental mapping of element Au exhibits similar networks to the interconnected ligaments in the SEM images. Although, relatively uniform distributions are observed in Co and O elements, implying the homogeneous deposition of CoO on any exposed surfaces of Au skeletons, as shown in Figures S3b–d.

To understand the information on the valence states in the NPG/CoO hybrid, XPS was conducted and the results are

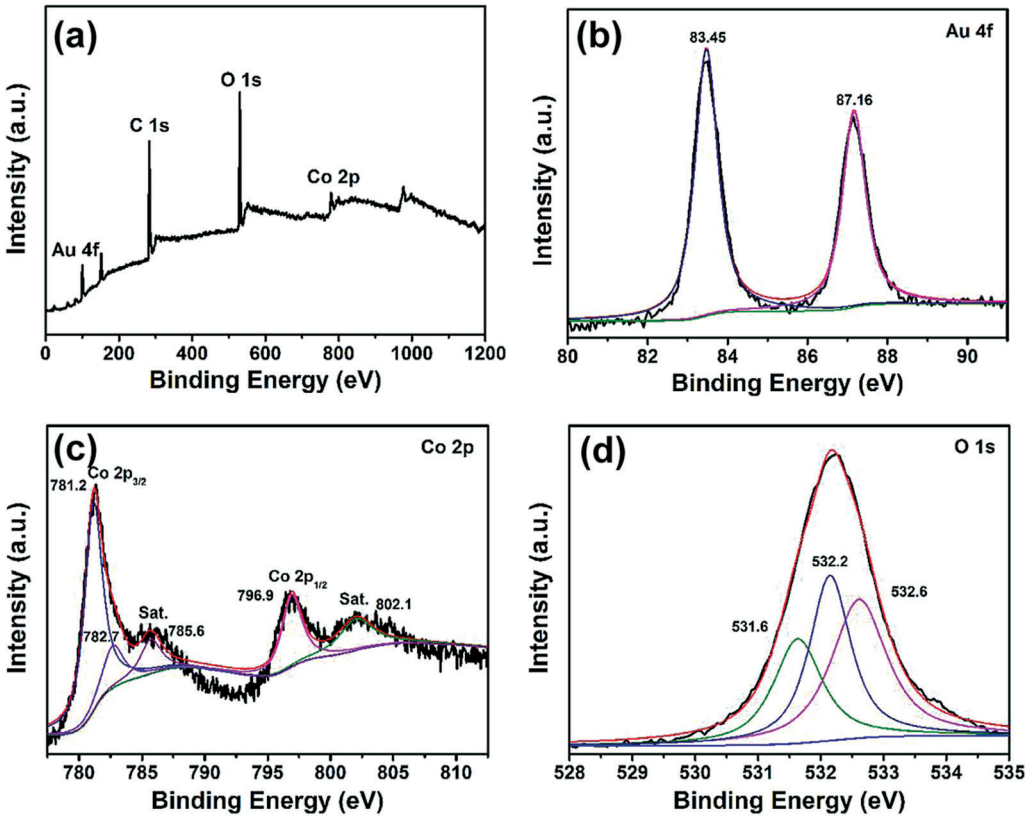

Figure 3. XPS spectra of NPG/CoO nanostructures: a) survey spectrum, b) Au 4f spectrum, c) Co 2p spectrum, and d) O 1s spectrum.

shown in Figure 3. Figure 3a shows the overall spectrum containing the composition information for the chemical bonds amongst Au, Co, O, and C elements. As shown in the Au 4f spectrum of the NPG/CoO electrode in Figure 3b, two Au 4f peaks (83.45 and 87.16 eV for $4f_{7/2}$ and $4f_{5/2}$, respectively) exhibited the zero-valent state of gold (Au), whereas gold oxide such as trivalent Au_2O_3 (85.9 eV for $4f_{7/2}$) does not exist. As shown in Figure 3c, the cobalt oxide exhibited two peaks corresponding to Co $2p_{3/2}$ in the lower binding-energy region (780–789 eV) and two peaks corresponding to Co $2p_{1/2}$ in the higher binding-energy region (794-805 eV). The Co $2p_{3/2}$ peak at 781.2 eV and Co $2p_{1/2}$ peak at 796.9 eV, with the corresponding satellite structure at 785.6 and 802.1 eV, can be ascribed to CoO species. The O 1s spectrum for the NPG/CoO sample shows three kinds of oxygen contributions in Figure 3d. The first peak (O1) at 531.6 eV is attributed to cobalt–oxygen bonds, the second one (O2) at 532.2 eV corresponds to hydroxyl groups, and the last peak (O3) at 532.6 eV is usually related to physical absorption and chemisorption of water molecules.

The square NPG/CoO pieces (0.2×1 cm^2) supported on the PET substrate were conducted with a three-electrode system, and the potentials are referred to a Ag/AgCl electrode. Figure 4a shows the cyclic voltammograms (CVs) of the NPG/CoO and NPG electrodes in aqueous electrolytes including 0.5 M KOH solution with 10 mM glucose at a scan rate of 20 mV s^{-1}. The CV of NPG/CoO has an analogous tendency with the pure NPG, except for the current density and the distinction of the two peaks. For the NPG/CoO hybrid, the small peak at 0.41 V almost vanishes in comparison with the pure NPG film, which might result from the synergistic effect of the NPG and CoO. To evaluate the electrocatalytic activities, depending on the loading level of CoO, the NPG/CoO hybrids were subjected to different numbers of deposition cycles from 100 to 800. If the electrochemical current for glucose oxidation is normalized by the macroscopic dimensions, it slightly increases with the thickening of the CoO shell, as shown in Figure 4b. When the cycle number is less than 200, the CoO shell usually holds the characteristic of the isolated islands rather than the continuous film. In this case, a larger number of Au/CoO interfaces can promote the electrochemical catalysis towards glucose oxidation. Therefore, a synergistic effect between Au and CoO can improve the catalytic performance of the nanoporous hybrid in comparison with the CV for pure CoO deposited on an indium tin oxide (ITO) substrate (Figure S4). With increase number of deposition cycles, the CoO shell becomes a continuous film, such that the CoO shell and the bare Au at the bottom can exhibit synergistic catalysis for glucose oxidation.

The amperometric current–time (*i*–*t*) curves of NPG/CoO hybrids upon sequential addition of glucose were also measured. Figure 4c illustrates the response current of glucose with various loaded electrodes at an applied potential of 0.26 V. The amperometric responses of the CoO-modified NPG electrode after 800 deposition cycles are larger than those of other NPG/

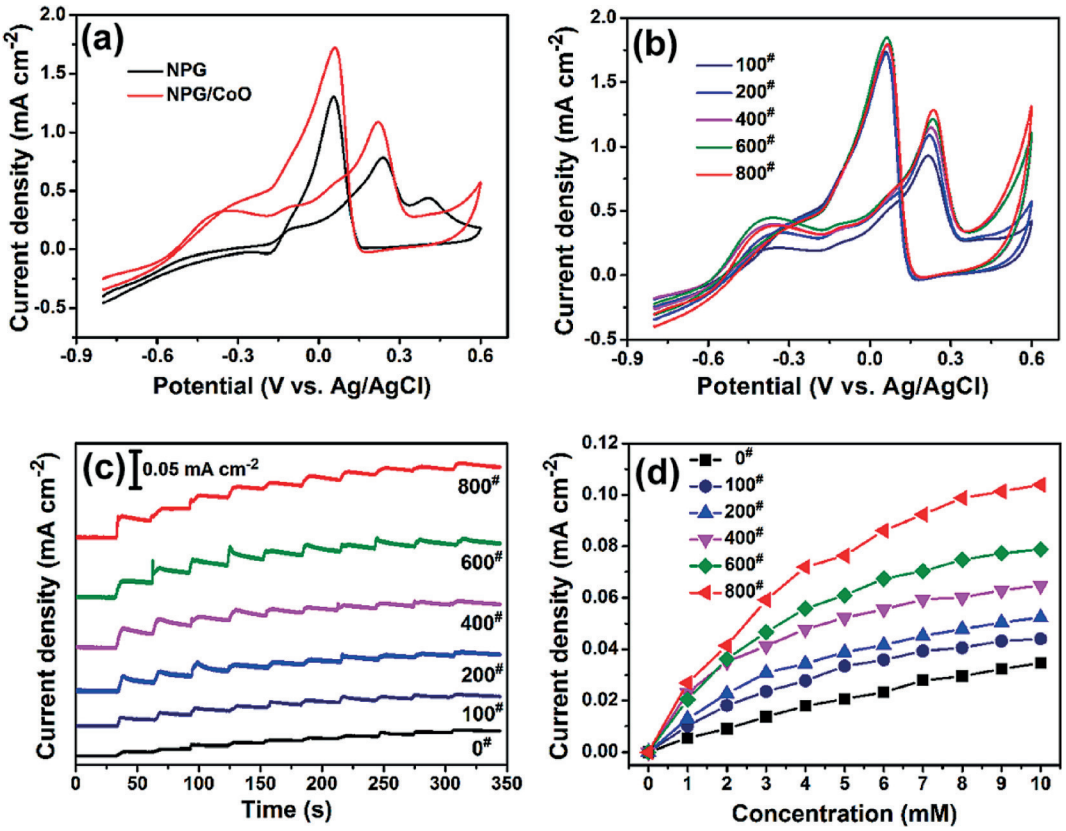

Figure 4. a) CVs of pure NPG and NPG/CoO in 0.5 M KOH with 10 mM glucose at a scan rate of 20 mV s^{-1}. b) CV curves of NPG after CoO deposition for different cycles measured at a potential scan rate of 20 mV s^{-1} in 0.5 M KOH with 10 mM glucose. c) Amperometric responses of the electrodes to sequential additions of 1 mM glucose into the stirred 0.5 M KOH solution. d) The corresponding calibration curves of NPG after CoO deposition for different numbers of cycles.

CoO electrodes and the pure NPG electrode, which could imply that the well-distributed CoO anchored on gold skeletons would provide more active sites for the catalytic redox reaction. The calibration curves for the NPG/CoO electrodes are shown in Figure 4d, and the electrocatalytic activity gradually increases with increasing CoO loading (from C100 to C800). It must be noted that NPG/CoO after 800 deposition cycles shows the maximum catalytic current. This tendency is related to the specific geometries and electron transport of the nanoporous hybrid.

To consider the electrochemical kinetics of these hybrid electrodes, electrochemical oxidation of glucose was performed during the CV sweeping measurements. Figure 5a shows the CVs of NPG/CoO based on the C800 electrode, performed in 0.5 M KOH solution containing 10 mM glucose at various scan rates of 10–100 mV s^{-1}. The calibration plot (Figure 5b) exhibits a good linear relationship between the current density and the scan rate, implying that the electrode reaction is a surface-controlled process. Upon the introduction of glucose, the electrochemical response of C800 to various concentrations of glucose (10–100 mM) was recorded, as shown in Figure 5c. A notable current increase at the anodic peak is observed in the CV recorded at a scan rate of 20 mV s^{-1}. The calibration curve of the corresponding amperometric response is shown in Figure 5d, revealing a linear relationship up to 100 mM of glucose ($R^2 = 0.9997$). This result suggests that the electrooxidation of glucose occurs with an outstanding sensitivity to the glucose concentration.

Besides electrochemical catalysis of glucose oxidization, the nanoporous NPG/CoO hybrid electrodes also exhibit high catalytic activity toward H_2O_2, which is useful for health diagnosis. Figure 6a shows CVs of the modified NPG/CoO electrode in the absence and presence of H_2O_2 in 0.1 M phosphate-buffered saline (PBS) at a scan rate of 20 mV s^{-1}. In blank PBS (pH 7.4), the CV of NPG/CoO does not display any visible peaks in the potential range from −0.8 to 0.6 V. In the presence of H_2O_2, a well-defined peak that is associated with the reduction of H_2O_2 can be observed at −0.3 V on NPG/CoO. Furthermore, with increasing concentration of H_2O_2 from 1.0 to 10 mM, the reduction current increases dramatically. Figure 6b represents the typical steady-state catalytic current of NPG/CoO in 0.1 M PBS with successive injection of H_2O_2 at an applied potential of −0.3 V (vs. Ag/AgCl). It is clear that the current increases linearly with increasing concentration of H_2O_2 up to 92.9 mM ($R^2 = 0.9983$). From the slope of the calibration curve, as shown in Figure 6c, the sensitivity of the NPG/CoO electrode for H_2O_2 was determined to be 0.0625 mA mM^{-1} cm^{-2}. Though the thickness of the NPG/CoO electrode is 100 nm, the sensitivity of the ultrathin NPG/CoO electrode is comparable to that of those using graphene sheets, noble metals, and metal oxide nano-

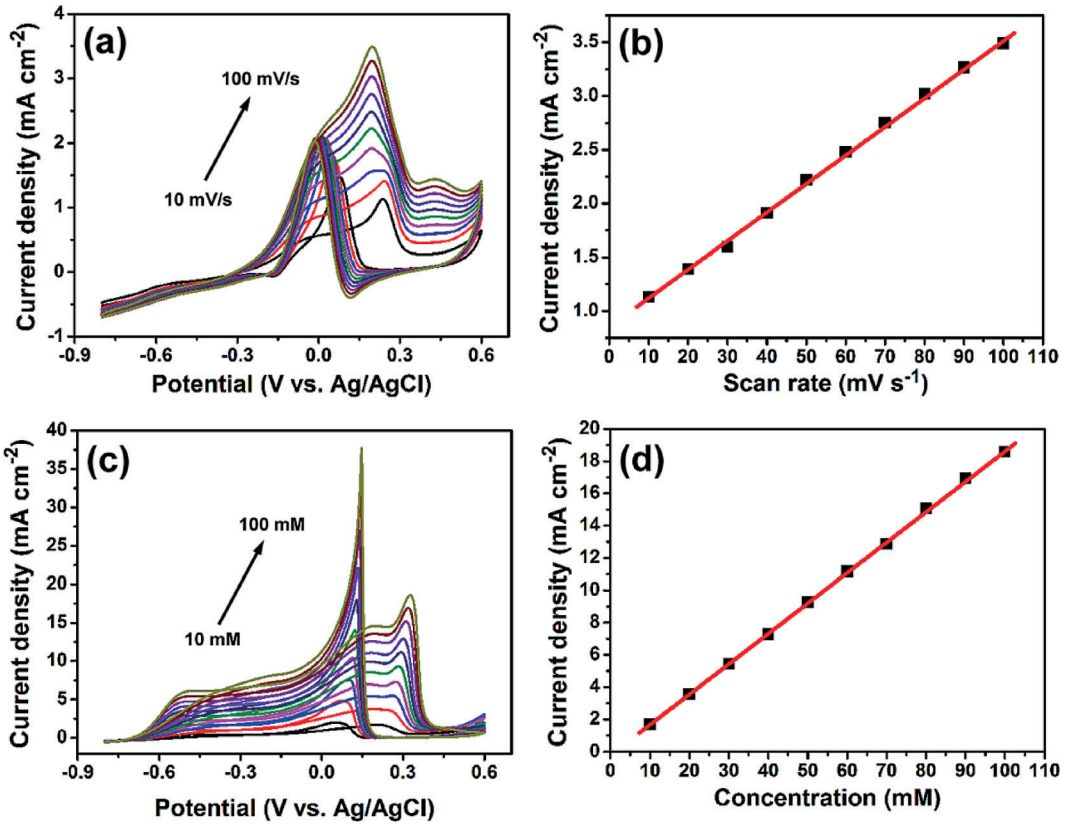

Figure 5. a) CVs of the NPG/CoO electrode in 0.5 M KOH solution with 10 mM glucose at various scan rates (10–100 mV s^{-1}). b) Plots of the oxidation peak current versus scan rate. c) CVs of the NPG/CoO electrode in 0.5 M KOH solution with different amounts of glucose at a scan rate of 20 mV s^{-1}. d) Calibration plot of oxidation peak current versus glucose concentration.

particles as composite electrodes.[14,16] This can be attributed to the superior electrocatalytic activity of the CoO shell towards H_2O_2. Furthermore, the NPG also increases the effective surface area and has the capacity to promote electron-transfer reactions. With ALD of the CoO shell onto the Au skeleton, the NPG/CoO electrode offers a fast and sensitive electrochemical electrode to monitor the H_2O_2 level in medical clinics. The detection limit of the NPG/CoO hybrid electrode is 0.1 mM, as shown in Figure S5. To consider the selectivity of the NPG/CoO hybrids, the potential interferences of several foreign species in real cells, including ascorbic acid (AA) and dopamine (DA), were investigated. The amperometric responses of the NPG/CoO at an applied potential of −0.3 V were investigated with the continuous addition of 0.5 mM H_2O_2, 0.1 mM AA, and 0.1 mM DA. Figure 6d shows the electrical responses of interferences during H_2O_2 detection. The results show that the NPG/CoO electrode has much weaker responses from AA and DA than from H_2O_2, which indicates that the presence of these species will not significantly affect the quantitative detection of H_2O_2. The interference test demonstrated that the NPG/CoO sensor was highly specific to H_2O_2, even in the presence of common interfering species.

3. Conclusions

We successfully fabricated a flexible NPG/CoO electrode with open and continuous porosity by using an ALD deposition approach and explored its application as an electrode material for electrochemical catalysis. Owing to the synergy effect of NPG and CoO in the composite, the resultant NPG/CoO-based electrode shows significantly improved electrochemical catalysis performance for glucose and H_2O_2. This novel NPG/CoO composite exhibits high catalysis activity for glucose as well as excellent sensitivity and selectivity for the detection of H_2O_2, which holds unique promise for applications in nonenzymatic H_2O_2 biosensors. Therefore, it is envisioned that the fabrication of NPG/CoO provides a blueprint for designing various nanoporous metal/transitional-metal oxide composite structures, which is promising for a wide range of applications in catalysis and biosensing.

Experimental Section

Fabrications of Porous NPG/CoO Hybrids

All chemicals were used as received without any further purification. Free-standing NPG leaf, with dimensions of 10 mm × 20 mm × 100 nm, was fabricated by de-alloying a commercial $Au_{35}Ag_{65}$ film in concentrated HNO_3 solution (70% in weight percentage) for 8 h at room temperature. Chemical contaminations on the surface

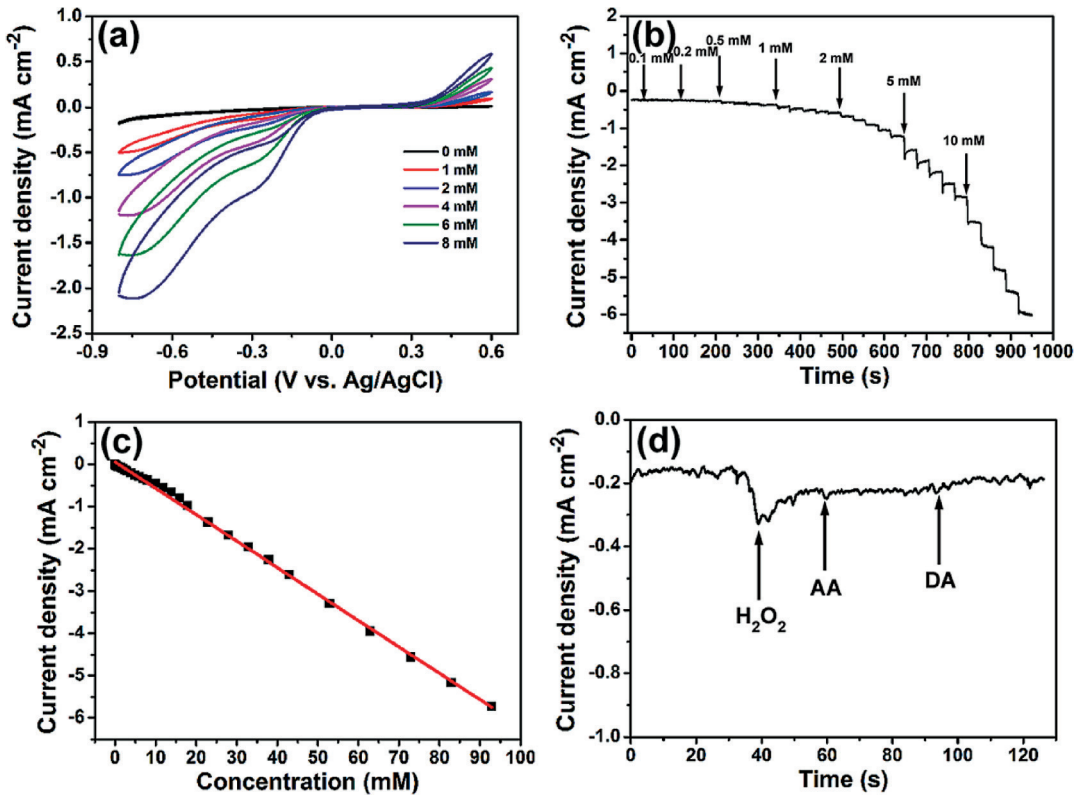

Figure 6. a) CVs of the NPG/CoO electrode in 0.1 M PBS with different amounts of H_2O_2 at a scan rate of 20 mV s^{-1}. b) Amperometric response curve of the NPG/CoO electrode at a potential of −0.3 V versus Ag/AgCl in stirred 0.1 M PBS upon continuous injection of H_2O_2 droplets. c) Calibration curve of the amperometric sensor as a function of H_2O_2 concentration. d) Effect of interfering species on the biosensor response.

were rinsed off by floating the sample on pure water (18.2 MΩ cm) for 30 min. The as-prepared NPG film was transferred onto a PET substrate. Subsequently, the CoO layer was deposited by using ALD (SUNALE R200 reactor). Chemical precursors were bis(cyclopentadienyl)cobalt(II) [Co(Cp)2, 98%, Strem Chemicals) and O_3 (ca. 11% by volume]. High-purity nitrogen (99.999%) was used as the source carrier and purging gas. The bis(cyclopentadienyl)cobalt(II) was evaporated at 100 °C, and the chamber temperature was kept at approximately 150 °C to ensure geometric stability of the PET substrate. The thickness of the CoO layer was tailored by adjusting the number of deposition cycles.

Microstructure Characterization

Characterization of the microstructure was carried out in a field-emission scanning electron microscope (JSM7600F) and a field-emission transmission electron microscope (JEOL2100). Element mapping of NPG/CoO was carried out by using EDS produced by Oxford Instruments. XPS was measured on a PerkinElmer model PHI 5600 XPS system with a resolution of 0.3–0.5 eV from a monochromatic Al anode X-ray source with Kα radiation (1486.6 eV).

Electrochemical Measurements

All electrochemical measurements were carried out on a CHI660D electrochemical workstation with a conventional three-electrode system at room temperature. The NPG/CoO hybrid was the working electrode, a platinum foil was used as the counter electrode, and a Ag/AgCl electrode was utilized as the reference to calibrate the potential. Prior to the evaluation of electrochemical catalysis, the electrolytes were purged with high-purity nitrogen (99.999%) for 30 min to remove the oxygen in the electrolyte.

Acknowledgements

This work was partially supported by Innovation Funding of HUST for International Collaborations (2014ZZGH018), National Basic Research Program of China (2013CB934800), Specialized Research Fund for the Doctoral Program of Higher Education (20130142120089), Hubei Province Funds for Distinguished Young Scientists (2015CFA034), Program for Changjiang Scholars and Innovative Research Team in University (IRT13017), and National Science Foundation of China (51371084, 51173055, 51575217).

Keywords: atomic layer deposition · biosensors · cobalt monoxide · electrochemical catalysis · nanoporous gold

[1] F. X. Xiao, S. F. Hung, J. W. Miao, H. Y. Wang, H. B. Yang, B. Liu, *Small* **2015**, *11*, 554 – 567.
[2] M. S. A. Sher Shah, A. R. Park, K. Zhang, J. H. Park, P. J. Yoo, *ACS Appl. Mater. Interfaces* **2012**, *4*, 3893 – 3901.
[3] H. T. Yu, X. Quan, S. Chen, H. M. Zhao, Y. B. Zhang, *J. Photochem. Photobiol. A* **2008**, *200*, 301 – 306.
[4] S. Xiao, F. Xiao, Y. Hu, S. L. Yuan, S. Wang, L. H. Qian, Y. Q. Liu, *Sci. Rep.* **2014**, *4*, 4370.
[5] S. J. Guo, S. Zhang, L. H. Wu, S. H. Sun, *Angew. Chem. Int. Ed.* **2012**, *51*, 11770 – 11773; *Angew. Chem.* **2012**, *124*, 11940 – 11943.
[6] B. Šljukić, C. E. Banks, R. G. Compton, *Nano Lett.* **2006**, *6*, 1556 – 1558.

[7] Y. Y. Liang, Y. G. Li, H. L. Wang, J. G. Zhou, J. Wang, T. Regier, H. J. Dai, *Nat. Mater.* **2011**, *10*, 780 – 786.
[8] H. L. Jiang, T. Akita, T. Ishida, M. Haruta, Q. Xu, *J. Am. Chem. Soc.* **2011**, *133*, 1304 – 1306.
[9] J. L. Kang, L. Y. Chen, Y. Hou, C. Li, T. Fujita, X. Y. Lang, A. Hirata, M. W. Chen, *Adv. Energy Mater.* **2013**, *3*, 857 – 863.
[10] F. Xiao, J. B. Song, H. C. Gao, X. L. Zan, R. Xu, H. W. Duan, *ACS Nano* **2012**, *6*, 100 – 110.
[11] Y. S. Hu, Y. G. Guo, W. Sigle, S. Hore, P. Balaya, J. Maier, *Nat. Mater.* **2006**, *5*, 713 – 717.
[12] C. Zhang, L. Qian, K. Zhang, S. Yuan, J. Xiao, S. Wang, *J. Mater. Chem. A* **2015**, *3*, 10519 – 10525.
[13] X. Y. Lang, H. Y. Fu, C. Hou, G. F. Han, P. Yang, Y. B. Liu, Q. Jiang, *Nat. Commun.* **2013**, *4*, 2169.
[14] J. B. Xi, Y. Zhang, N. Wang, L. Wang, Z. Y. Zhang, F. Xiao, S. Wang, *ACS Appl. Mater. Interfaces* **2015**, *7*, 5583 – 5590.
[15] X. X. Xiao, M. Wang, H. Li, Y. C. Pan, P. C. Si, *Talanta* **2014**, *125*, 366 – 371.
[16] S. J. Li, J. M. Du, J. P. Zhang, M. J. Zhang, J. Chen, *Microchim. Acta* **2014**, *181*, 631 – 638.
[17] X. Wang, W. Tian, T. Y. Zhai, C. Y. Zhi, Y. Bando, D. Golberg, *J. Mater. Chem.* **2012**, *22*, 23310 – 23326.
[18] Q. Z. Jiao, M. Fu, C. You, Y. Zhao, H. S. Li, *Inorg. Chem.* **2012**, *51*, 11513 – 11520.
[19] H. Y. Jin, J. Wang, D. F. Su, Z. Z. Wei, Z. F. Pang, Y. Wang, *J. Am. Chem. Soc.* **2015**, *137*, 2688 – 2694.
[20] C. X. Xu, L. Q. Wang, R. Y. Wang, K. Wang, Y. Zhang, F. Tian, Y. Ding, *Adv. Mater.* **2009**, *21*, 2165 – 2169.
[21] X. Y. Lang, A. Hirata, T. Fujita, M. W. Chen, *Nat. Nanotechnol.* **2011**, *6*, 232 – 236.
[22] J. Ye, A. C. Baumgaertel, Y. M. Wang, J. Biener, M. M. Biener, *ACS Nano* **2015**, *9*, 2194 – 2202.
[23] Z. H. Li, Y. H. He, X. Ke, L. Gan, J. Zhao, G. F. Cui, G. Wu, *J. Power Sources* **2015**, *294*, 136 – 140.
[24] J. T. Zhang, P. P. Liu, H. Y. Ma, Y. Ding, *J. Phys. Chem. C* **2007**, *111*, 10382 – 10388.
[25] H. M. Yin, C. Q. Zhou, C. X. Xu, P. P. Liu, X. H. Xu, Y. Ding, *J. Phys. Chem. C* **2008**, *112*, 9673 – 9678.

Manuscript received: September 30, 2015
Accepted Article published: November 2, 2015
Final Article published: November 6, 2015